Induction of necroptosis in lung adenocarcinoma by miR-10b-5p through modulation of the PKP3/RIPK3/MLKL cascade

YING HU[1*], XIN LIU[2*], ZIHENG YUAN[1*], JIANPING HE[3], RUN MA[1], YUMING WANG[1] and GENFA YI[4]

[1]Department of Laboratory, The Second Affiliated Hospital of Kunming Medical University, Kunming, Yunnan 650101, P.R. China; [2]Department of Thoracic Surgery, The Second Affiliated Hospital of Kunming Medical University, Kunming, Yunnan 650101, P.R. China; [3]Department of Medical Genetics and Prenatal Diagnosis, Kunming Maternal and Child Health Centre, Kunming, Yunnan 650032, P.R. China; [4]Department of Medical Imaging, The First Affiliated Hospital of Kunming Medical University, Kunming, Yunnan 650051, P.R. China

Received October 16, 2024; Accepted February 20, 2025

DOI: 10.3892/or.2025.8889

Abstract. Globally, lung adenocarcinoma (LUAD) remains the leading cause of cancer-related mortality, highlighting the urgent need for innovative therapeutic approaches. Necroptosis has been recognized as a crucial mechanism for inhibiting cancer progression. Research has revealed a significant association between microRNA (miRNA)-mediated necroptosis and tumor progression. The present study aimed to elucidate the role and underlying mechanisms of miR-10b-5p in regulating necroptosis in the context of LUAD. In an investigation of LUAD, miRNA sequencing was conducted on both LUAD and adjacent non-tumor tissues, followed by the integration of external database information to identify specific target miRNAs. The expression of miR-10b-5p was verified in LUAD tissues and corresponding adjacent non-cancerous tissues using immunohistochemistry. *In vitro* experiments, utilizing LUAD cell lines engineered to modulate miR-10b-5p levels, assessed its effects on cellular activities and necroptosis. The inhibition of PKP3 by miR-10b-5p was determined using a dual luciferase reporter system. Furthermore, alterations in miR-10b-5p levels were found to affect PKP3 expression and inhibit the RIPK3/MLKL signaling pathway, as evidenced by western blot analysis in LUAD cell lines. The effect of PKP3 knockdown on cell activity and necroptosis in LUAD cell lines with low miR-10b-5p expression levels was assessed using cell function assays. Finally, a nude mouse xenograft model was used to investigate the effect of miR-10b-5p on LUAD growth *in vivo* and its specific mechanism of action. It has been revealed that miR-10b-5p levels are significantly elevated in LUAD specimens. Further investigations demonstrated that an increase in miR-10b-5p enhances the proliferation of LUAD cells and suppresses the progression of necroptosis, as evidenced by *in vitro* experiments. Through dual luciferase reporter assays, PKP3 was confirmed as a direct target negatively regulated by miR-10b-5p, leading to reduced expression levels. Western blot analysis indicated that miR-10b-5p inhibits the RIPK3/MLKL pathway activation through downregulation of PKP3, which leads to increased cell proliferation and decreased necroptosis. However, knockdown of PKP3 reversed the inhibitory effect of miR-10b-5p inhibitors on cellular activity and inhibited necrosis by suppressing the RIPK3/MLKL signalling pathway. In addition, animal model studies demonstrated that inhibition of miR-10b-5p activated the RIPK3/MLKL pathway by promoting PKP3 expression and significantly reduced LUAD growth by promoting necroptosis. In conclusion, our studies have revealed that the miR-10b-5p functions as a tumorigenic factor, enhancing various cellular activities in LUAD cells and suppressing necroptosis by specifically targeting PKP3, thereby inhibiting activation of the RIPK3/MLKL pathway. Importantly, interventions using inhibitors that specifically target miR-10b-5p have shown significant success in impeding the progression of LUAD by promoting necroptosis in both cellular and animal models. Thus, targeting miR-10b-5p holds considerable potential as a therapeutic strategy for LUAD.

Correspondence to: Professor Yuming Wang, Department of Laboratory, The Second Affiliated Hospital of Kunming Medical University, 374 Dianmeng Avenue, Wuhua, Kunming, Yunnan 650101, P.R. China
E-mail: wangym992011@163.com

Professor Genfa Yi, Department of Medical Imaging, The First Affiliated Hospital of Kunming Medical University, 374 Dianmeng Avenue, Wuhua, Kunming, Yunnan 650051, P.R. China
E-mail: genfa@kmmu.edu.cn

*Contributed equally

Key words: lung adenocarcinoma, microRNA-10b-5p, necroptosis, PKP3, RIPK3/MLKL

Introduction

Globally, lung cancer has emerged as the predominant malignant tumor with the highest rates of incidence and mortality, experiencing a notable increase in the past 50 years (1). The classification of this cancer predominantly includes non-small cell lung cancer (NSCLC) and small cell lung cancer (SCLC). Among NSCLC types, lung adenocarcinoma (LUAD) emerges as the most commonly identified pathological

subtype, accounting for ~40% of all lung cancer diagnoses, with an incidence that continues to escalate (2). LUAD, which often lacks distinct early clinical manifestations, tends to exhibit high metastatic capacity from the onset, leading to a grim prognosis with 5-year survival rates <20% (3,4). Despite the significant advances in molecularly-targeted therapies, the long-term outcomes for LUAD remain suboptimal (5). Identifying unique tumor markers and novel therapeutic strategies, enhancing early detection through systematic screening, and fostering the development of precise and early intervention treatments are imperative to enhance survival outcomes for patients with LUAD.

The armadillo protein family includes several plakophilins (PKPs), specifically PKP1, PKP2 and PKP3, which are integral to its structure. These proteins are involved in the formation of bridging granules, playing a pivotal role in promoting intercellular adhesion and communication. Alterations in PKP3 expression are implicated in various human pathologies, particularly cancers (6). Emerging studies highlight that the function of PKP3 can oscillate between a tumor suppressor role and oncogenic activity, depending on the stage and type of the cancer. Notably, heightened levels of PKP3 are associated with an enhancement in cell proliferation, migration and invasion in specific types of cancer such as pancreatic, ovarian and NSCLC (7-9). Conversely, a reduction in PKP3 expression in colon and bladder cancers correlates with poorer prognoses (10,11). These findings indicate the dual and variable impact of PKP3 within different cancer contexts. Previous studies have shown that elevated PKP3 levels correlate with adverse outcomes in NSCLC, enhancing tumor cell migration, invasion and immune escape (9,12-14). However, the specific mechanisms through which PKP3 influences LUAD, a prevalent NSCLC subtype, remain to be elucidated.

Programmed cell death (PCD) is governed by genetic regulation. Traditionally, apoptosis, which relies on cysteine asparaginase, was regarded as the sole PCD pathway. As research progresses, more types of PCD are gradually being identified, including necroptosis (15). Fundamentally differing from apoptosis, necroptosis is independent of cysteine asparaginase and demonstrates characteristics similar to those of necrosis, including increased cellular volume, swelling of organelles, rupture of the plasma membrane, and the subsequent expulsion of cellular constituents (16). The regulation of necroptosis is stringent, requiring the activation of receptor-interacting protein (RIP) kinases such as RIPK1 and RIPK3, along with the involvement of the mixed lineage kinase domain-like protein (MLKL), which acts as a substrate for RIPK3 (17). This mode of cell death releases damage-associated molecular patterns, which enhance antitumor immune responses and may trigger further immune functions. Evidence increasingly supports the idea that modulation of the necroptosis signaling pathway could provide a viable strategy for cancer therapy. Nonetheless, cancer cells often enhance their survival by modulating genes associated with necroptosis, such as by reducing RIPK3 expression levels. The exact regulatory mechanisms governing necroptosis in LUAD remain unclear.

MicroRNAs (miRNAs or miRs) are small RNA molecules that lack coding capability and exhibit significant conservation across species. They play a crucial role in modulating diverse cellular activities, either by regulating protein synthesis or facilitating the degradation of mRNA (18). These miRNAs participate in the regulation of PCD, which includes apoptosis, autophagy and necroptosis. However, the literature provides limited details on the specific mechanisms through which miRNAs influence necroptotic cell death (19). According to studies conducted by Harari-Steinfeld *et al* (20), miR-675 enhances necroptosis in hepatocellular carcinoma cells by inhibiting the Fas-associated protein with death domain (FADD), a key mediator in apoptotic signaling. By contrast, research by Li *et al* (21) indicated that miR-204-3p reduces necroptosis pathways, specifically MAPK and RIP1/MLK1, leading to decreased proliferation and increased apoptosis in gastric cancer cells. Elevated levels of miR-10b-5p have increasingly been associated with worse patient outcomes in various cancers, including gastric and hepatocellular carcinomas, as well as glioma (22-24). However, the impact of miR-10b-5p on necroptosis pathways in tumor cells remains unexplored.

The current investigation provides initial evidence through both *in vivo* and *ex vivo* studies that miR-10b-5p acts as an oncogene. It inhibits the activation of the RIPK3/MLKL signalling pathway by directly targeting PKP3, thereby promoting tumour proliferation and inhibiting necroptosis development. Notably, reducing miR-10b-5p levels curbed the progression of LUAD by facilitating necroptosis. These findings elucidate the molecular mechanisms underlying LUAD and highlight miR-10b-5p as a promising target for innovative therapeutic strategies.

Materials and methods

Tissue samples. Over the course of 1 year, from July 2022 to July 2023, the Department of Thoracic Surgery at The Second Affiliated Hospital of Kunming Medical University (KMUH) collected tissue samples from six patients diagnosed with LUAD and were receiving treatment, three of whom were female and three of whom were >60 years old. These samples included both cancerous tissues and adjacent non-tumorous tissues. Each specimen was confirmed as LUAD through histopathological evaluation. After collection, all samples were immediately immersed in liquid nitrogen to ensure rapid freezing and were then stored at -80˚C for further examination. The research protocols adhered to the ethical guidelines of the Declaration of Helsinki and were approved by the KMUH Ethics Committee (approval no. PJ-2024-125; Kunming, China). Written informed consent was obtained from all participants.

Cell lines and cell culture. Both A549 and 293FT cell line was procured from Brick Bio (https://www.brickbio.com), and cultured using F-12K and DMEM medium (Gibco; Thermo Fisher Scientific, Inc). This medium was supplemented with fetal bovine serum at a 10% concentration and a 1% solution of penicillin-streptomycin, with both additives sourced from Gibco; Thermo Fisher Scientific, Inc. The protocol required the exclusive use of F-12K medium. After 293FT cells were used as tool cells for lentiviral packaging, they were cultured in IMDM medium containing 10% fetal bovine serum and 1% PSG. Both types of cells were cultured in an incubator at 5% CO_2 concentration and 37˚C. Selection for further experimental

use was restricted to cells that demonstrated vigorous growth during the logarithmic phase.

MiRNA differential expression analysis. Fresh LUAD tissues, along with their matched non-cancerous counterparts, were procured and classified into two categories: One comprising LUAD tissues and the other consisting of the adjacent non-malignant tissues. Three samples from each group were randomly selected for sequencing. The tissue samples were cut into fragments <0.5 cm, stored in an insulated container filled with dry ice, and dispatched to Shanghai Ouyi Biomedical Technology Co., Ltd. for processing. RNA extraction, quantification and quality assessment were performed by the same company. Following successful library quality checks, sequencing was carried out on the Small RNA platform (illumina Hiseq X ten, illumina Co., Ltd.). Differentially expressed miRNAs (DEmiRNAs) between LUAD and paracancerous tissues were identified using the 'Lima' software package in R (https://CRAN.R-project.org/package=limma), based on the sequencing data with |log2FC| ≥2 and FDR<0.05 as selection criteria. The 'ggplot2' package was employed to create a volcano plot of these DEmiRNAs. Multiple databases, including TargetScan Human 7.2 (https://www.targetscan.org/vert_72/), Starbase (https://rnasysu.com/encori/), miRWalk (http://mirwalk.umm.uni-heidelberg.de/) and miRmap (https://mirmap.ezlab.org/), were used to identify miRNAs that potentially bind to the PKP3 target. miRNAs confirmed in each database as having a target-binding relationship were cross-referenced with those identified through sequencing.

Cell transfection. From the 3rd to 5th generations post-recovery, A549 cells exhibiting robust growth were selected for experiments. The cells were dissociated into a single-cell suspension using trypsin digestion, followed by one to two phosphate-buffered saline (PBS) washes and subsequent cell quantification. Prior to plating, the concentration of the cell suspension was adjusted to $2x10^5$/ml, and the suspension was then dispensed into 24-well plates to ensure a confluence of 30-50% at the onset of transfection. During the transfection process, a miRNA mimic (UACCCUGUAGAACCGAAUUUGUG) was first diluted by mixing 1.25 μl of a 20 μM stock solution into 30 μl of 1X riboFECT™ CP Buffer with gentle stirring. A total of 3 μl of riboFECT™ CP Reagent (Guangzhou RiboBio Co., Ltd.) were introduced into the solution, followed by gentle pipetting to mix. The mixture was allowed to stand at room temperature for 15 min. Afterward, the mixture was combined with serum-free medium, and the setup was incubated at 37˚C within a CO_2 incubator for 48 h to facilitate subsequent experimental procedures.

PKP3 lentiviral transfection was performed using 293T cells, interfering lentivirus and PGMLV-ZsGreen1-Puro vector control. Interfering lentivirus and PGMLV-ZsGreen1-Puro vector control was purchased from Honorgene (https://www.honorgene.com). The lentivirus was constructed by Shanghai Jiman Biotechnology Co. Ltd. using a second-generation viral packaging system, and the lentiviruses, packaging plasmids, and envelope plasmids used were vsvg, gag, and rev, respectively. In a 6-well plate, A549 cells were seeded at a density of $3x10^5$ cells per well. Upon achieving ~70% confluence, the original culture medium was replaced with 1 ml of fresh medium containing 8 μg/ml of polyethylene glycol, sourced from Beijing Solarbio Science & Technology Co., Ltd. Concurrently, 10 μg of lentiviral plasmid was added to each well to achieve multiplicity of infection (MOI)=5. After 72 h of infection at 37˚C, cells expressing green fluorescent protein were visible under a fluorescence microscope. The medium was then replaced with selection medium containing 4 μg/ml puromycin from Beijing Solarbio Science & Technology Co., Ltd., which allowed for 1-2 generations of selection to establish stable cell lines. The cultures were propagated at a constant temperature of 37˚C within a cell culture incubator maintained at 5% CO_2 and optimal humidity levels.

Reverse transcription-quantitative PCR (RT-qPCR). Total RNA was isolated employing TRIzol reagent (Thermo Fisher Scientific, Inc.). Spectrophotometry was utilized to assess the purity and concentration of the extracted nucleic acids. For converting RNA into cDNA, the following kits were used according to the manufacturers' protocols: the FastKing RT Kit (With gDNase) from Tiangen Biotech Co., Ltd., or the Bulge-Loop miRNA RT-qPCR Starter Kit (Guangzhou RiboBio Co., Ltd.,) were selected. For RT-qPCR analysis targeting both mRNA and miRNA, the Taq Pro Universal SYBR qPCR Master Mix and the SYBR Green Mix (Invitrogen; Thermo Fisher Scientific, Inc.) were applied. According to the manufacturer's instructions, thermocycling conditions were as follows: mRNA, pre-denaturation at 95˚C for 30 sec, 40 cycles at 95˚C for 10 sec, 60˚C for 30 sec; miRNA: pre-denaturation at 95˚C for 10 min, 40 cycles at 95˚C for 2 sec, 60˚C for 20 sec, 70˚C for 10 sec. The primer sequences are detailed in Table SI. The relative gene expression was quantified using the $2^{-\Delta\Delta Cq}$ method (25), with GAPDH serving as the internal reference gene.

Immunoblotting. Tissue samples or cells from tumors were lysed using RIPA buffer (Shanghai Beyotime Co., Ltd.), followed by centrifugation to extract total proteins. Protein concentrations were determined using an IMPLEN Ultra-Micro Spectrophotometer (measuring absorbance at 280 nm). After quantification, proteins were separated by SDS-PAGE through a 4% concentrate gel (adjust the amount of protein sampled to 40 μg per lane) and transferred electrophoretically to PVDF membranes (MilliporeSigma). The membranes were blocked with 5% non-fat milk for 2 h at ambient temperature, followed by overnight incubation at 4˚C with primary antibodies: PKP3 (1:2;000; cat. no. 109441), PCNA (1:2,000; cat. no. 92552), Ki67 (1:1,000, cat. no. 16667), Bax (1:2,000; cat. no. 32503), Bcl-2 (1:2,000; cat. no. 182858), Caspase-3 (1:2,000; cat. no. 184787; all from Abcam), RIPK3 (1:1:1,000, cat. no. 10188), phosphorylated (p)-RIPK3 (1:1,000, 91702), MLKL (1:1,000; cat. No 14993), p-MLKL (1:1,000, cat. no. 18640), Caspase-8 (1:1,000, cat. no. 9746; all from Cell Signaling Technology, Inc.) and GAPDH (1:2,000, cat. no. OTI2D9; OriGene Technologies, Inc.). Membranes were then incubated with HRP-conjugated secondary antibodies (goat anti-rabbit; 1:4,000, cat. no. GB13063-50; Wuhan Servicebio Technology Co., Ltd.; goat anti-mouse; 1:4,000, M21001S; Abmart Pharmaceutical Technology Co., Ltd.) for 2 h at room temperature. Protein bands were visualized using an Enhanced Chemiluminescence (ECL) System

Kit (Thermo Fisher Scientific, Inc.). Final analysis was performed using ImageJ software (version 1.50b; National Institutes of Health).

Dual-luciferase reporter assay. To investigate the specific interaction between miR-10b-5p and the PKP3 3'-untranslated region (UTR), the region predicted to contain the miR-10b-5p binding site was amplified and subsequently cloned into the pGL3 control vector (Promega Corporation). This construct was introduced into A549 cells via co-transfection with either a miR-10b-5p mimic or a NC mimic using Lipofectamine™ 3000 (Thermo Fisher Scientific, Inc.). Wild-type (WT) and mutant (MUT) versions of the PKP3 reporter plasmid, which included modifications at the miR-128 binding site, were generated using the QuikChange II Targeted Mutation Kit (Agilent Technologies, Inc.), following the manufacturer's protocol. Relative luciferase activity was measured 48 h post-transfection utilizing the dual luciferase reporter assay system from Promega Corporation, following the protocol recommended by the manufacturer. The experimental precision was upheld by comparing the luminescence readings of firefly luciferase (fLuc) and *Renilla* luciferase (rLuc), expressed as relative light units. By utilizing Renilla luciferase as a control, the activation of the target gene was analyzed by calculating the ratio of luminescence between fLuc and rLuc across different samples.

Cell Counting Kit-8 (CCK-8). To assess the viability of T cells, the CCK-8 assay was utilized (Shanghai Beyotime Co., Ltd.). A549 cells were subjected to 0.25% trypsin for digestion, collected, and the supernatant was removed. The cells were resuspended in 1 ml of complete medium. Following enumeration, the cells were plated at a density of 5,000 cells per well in 96-well plates, with triplicate samples for each experimental group. When cell confluence reached ~80%, transfections were carried out for 24 h. After this period, 10 μl of CCK-8 solution was added to each well. The plates were then incubated in the dark at 37˚C for 2 h. OD was measured at 450 nm using a microplate reader. Cell viability percentage was calculated with the formula: (OD of experimental wells-OD of blank wells)/(OD of control wells-OD of blank wells) x100%.

Colony formation assay. Cells were inoculated into 6-well plates (500 cells/well) and cultured at 37˚C, 5% CO_2 and 90% relative humidity for 2 weeks, and then fixed with 4% paraformaldehyde (PFA) solution at ambient temperature (Shanghai Aladdin Biochemical Technology Co., Ltd.) and stained with 0.1% crystal violet staining solution at ambient temperature (Beijing Solarbio Science & Technology Co., Ltd.) for 10 min. The staining solution was then gently rinsed with tap water, and the images were captured to record the cellular clone formation. When each clone is >50 cells, it can be stained for observation and subsequently images can be captured for manual counting. Rate of clone formation (%) was determined using the following formula: number of cell clones/number of inoculated cells x100%.

Apoptosis detection. Apoptosis assays were performed using flow cytometry techniques. A549 cells were enzymatically digested, and aliquots of 30,000 cells were dispensed into each well of 12-well plates. Triplicate wells were prepared for each experimental condition. After reaching the logarithmic phase growth, apoptosis was assessed 24 h post-transfection. Additionally, three control groups were established: A blank control, a PI single positive control, and a FITC single positive control. To facilitate resuspension, 400 μl of Binding Buffer was added to each tube. Subsequently, 400 μl of Binding Buffer was added to resuspend the cells. To the experimental wells, 5 μl of FITC dye was added and incubated for 15 min, followed by the addition of 10 μl of PI dye. After an additional 5-min incubation, apoptosis was quantified by flow cytometry (Novocyte 2060Rl ACEA Bioscience, Inc.) using the NovoExpress software (version 1.6.2; Agilent Technologies, Inc.).

Tumor xenograft experiment. A total of 21 male BALB/c nude mice, 4-6 weeks old, averaging 19.5 g, were obtained from Kunming Medical University (Yunnan, China). The mice were housed in an SPF-grade sterile laminar flow chamber, with a controlled humidity level of 55±5% and temperatures ranging from 22-25≥C. They had free access to water and were fed a standard laboratory diet. Cells were subjected to trypsin treatment until they became rounded but remained attached to the culture dish. After trypsin removal, a serum-free medium was added to prepare a cell suspension. This suspension was then centrifuged at at 1,200 x g for 5 min under ambient conditions, rinsed once, and resuspended in PBS to a final concentration of $1x10^5$ cells/ml. Each mouse received a subcutaneous injection at a vascular-rich site on the upper right waist. After the first injection, the mice were handled routinely following three inoculations, with 1-day intervals between each. The weight of the mice and the volume of subcutaneous tumors were documented; the length and maximum diameter of the tumors were measured to plot growth curves. A total of 5 weeks after inoculation, mice were euthanized by cervical dislocation, subcutaneous tumours were removed, weighed, and images were captured. Tumor dimensions were carefully recorded before the samples were immediately preserved by freezing in liquid nitrogen, then stored at -80˚C for subsequent molecular analyses. A subset of these tumor samples was randomly selected for further analysis; half were fixed for 1 h at ambient temperature in 2.5% glutaraldehyde for electron microscopy, while the remainder were fixed for 30 min at ambient temperature in 4% paraformaldehyde for morphological studies. The experimental protocol was approved by the KMUH Animal Care Committee (approval no. kyfeyxm2024127; Kunming, China).

TUNEL staining. Sections of paraffin-embedded subcutaneous graft tumor samples, measuring 4 μm in thickness, underwent deparaffinization with xylene followed by rehydration via graduated ethanol solutions. Proteinase K, free of DNase and at a concentration of 20 μg/ml, was incrementally added and then incubated at 42˚C for a period of 25 min. To quench the activity of endogenous peroxidase, tissues were treated with a 3% solution of hydrogen peroxide for 20 min at ambient temperature. Following the manufacturer's guidelines, TdTase was combined with Biorin-dUTP at a ratio of 1:9 to ensure thorough integration before application. The mixture of Biorin-dUTP was then applied in a stepwise manner and incubated in obscurity at 37˚C for 60 min. The

process was terminated by adding a stopping solution and permitting an additional incubation of 10 min at ambient temperature. An incremental addition of streptavidin-HRP solution was performed, followed by a 30-min incubation at ambient temperature. Thereafter, the sections underwent stain development using DAB chromogenic substrate. To finalize the process, the samples were stained with hematoxylin for a duration of 5 min and then differentiated with 1% hydrochloric acid in ethanol. The slides underwent subsequent dehydration, clearing, and mounting as aforementioned, and finally observed using a light microscope with 5 fields of view per section and counted. The scale of the displayed images is both 1 and 2 microns.

Transmission electron microscopy (TEM). Subcutaneous graft tumor samples were segmented into blocks ranging from 0.5-1.0 mm^3 and subsequently immersed in a 2.5% glutaraldehyde solution for 1 h at ambient temperature for fixation. After trypsin digestion, the cells were centrifuged at 1,200 x g for 5 min under ambient conditions and rapidly immersed in an electron microscope fixative at 4˚C for 2-4 h. The samples underwent three washes, each utilizing 0.1 M PBS at pH 7.4, with each wash lasting 15 min. Following exposure to 1% osmium tetroxide until darkening occurred, the samples were washed with 1 M PBS for 10 min. Dehydration was carried out using progressively increasing concentrations of alcohol and acetone. After dehydration, the specimens were embedded in an appropriate medium. Ultrathin sections were then prepared for further analysis. The specimens were subjected to a dual staining process, first with uranyl acetate, followed by lead citrate, and were then allowed to air dry overnight at room temperature. Observations were conducted using transmission electron microscopy, and images were captured for further analysis.

Statistical analysis. Data were analysed using GraphPad Prism software version 10.02 (GraphPad Software; Dotmatics). Data from our study are presented as the mean ± SEM. Data obtained from at least three independent experiments were used for all analyses. Statistical analyses were performed by one-way ANOVA. Then, Bonferroni's multiple comparison test (for comparisons between more than 2 groups) or Student's t-test (for comparison of the two groups) was performed. $P<0.05$ was considered to indicate a statistically significant difference.

Table I. Differential miRNAs.

miRNA ID	Fold regulation	P-value
Upregulated		
hsa-miR-10b-5p	1.565	0.001387
hsa-miR-10b-3p	1.8817	0.000020
hsa-miR-200b-5p	1.97421	0.0005742
hsa-miR-365a-5p	2.4891	0.0008496
hsa-miR-135b-5p	3.069	0.000318
hsa-miR-135b-3p	3.307	0.0000356
hsa-miR-379-3p	3.618	0.001409
hsa-miR-105-5p	20.30	0.0000002
hsa-miR-1912-5p	24.168	0.000558
hsa-miR-1298-3p	23.34	0.039984
hsa-miR-767-5p	21.305	0.017374
hsa-miR-1298-5p	11.50	0.0000239
hsa-miR-205-5p	5.602	0.008949
hsa-miR-323a-3p	4.9766	0.001205
hsa-miR-1911-5p	10.46	0.004968
hsa-miR-431-5p	4.604	0.00092565
Downregulated		
hsa-miR-518a-3p	-5.868	0.001134
hsa-miR-30c-2-3p	-1.467	0.000267
hsa-miR-126-5p	-1.890	0.00005858
hsa-miR-486-5p	-1.976	0.000243
hsa-miR-126-3p	-2.040	0.0005586
hsa-miR-451a	-1.939	0.0002373
hsa-miR-135a-5p	-2.13	0.00003133
hsa-miR-144-5p	-2.102	0.0006989
hsa-miR-934	-2.407	0.0006117
hsa-miR-144-3p	-2.32	0.0000325
hsa-miR-486-3p	-2.47	0.00001277
hsa-miR-184	-2.675	0.0008835
hsa-miR-30a-5p	-1.870	0.000598
hsa-miR-873-5p	-3.07	0.000099
hsa-miR-516b-5p	-3.43	0.0000299

miRNA or miR, microRNA.

Results

miR-10b-5p screening in LUAD tissues. Sequencing analyses were performed on lung cancer samples and nearby non-malignant tissues to pinpoint miRNAs that display significant differences in expression in LUAD, utilizing a threshold of $P<0.05$ and an absolute log2FC >2. The study identified 16 miRNAs exhibiting increased expression and 15 displaying decreased expression in lung cancer specimens, as enumerated in Table I.

Following the analysis, histograms of differential miRNA and volcano plots were generated (Fig. 1A and B). Furthermore, heatmap analysis was performed to delineate the expression patterns of differential miRNAs in both the lung cancer and para-cancer groups (Fig. 1C). To elucidate the functions of the identified differential miRNAs, Gene Ontology (GO) and Kyoto Encyclopedia of Genes and Genomes (KEGG) pathway analyses were conducted. GO analysis highlighted that the primary biological functions of these miRNAs include inhibiting transcription via RNA polymerase II promoters; their cellular localization was mainly in the cytosol and the nucleus; additionally, their molecular roles were closely linked to binding of metal ions and DNA (Fig. 1D). Analysis through KEGG pathways showed that the miRNAs with varied expression significantly participated in pathways such as aldosterone-regulated sodium reabsorption, multiple autophagy mechanisms, Hedgehog signaling and 27 other pathways (Fig. 1E).

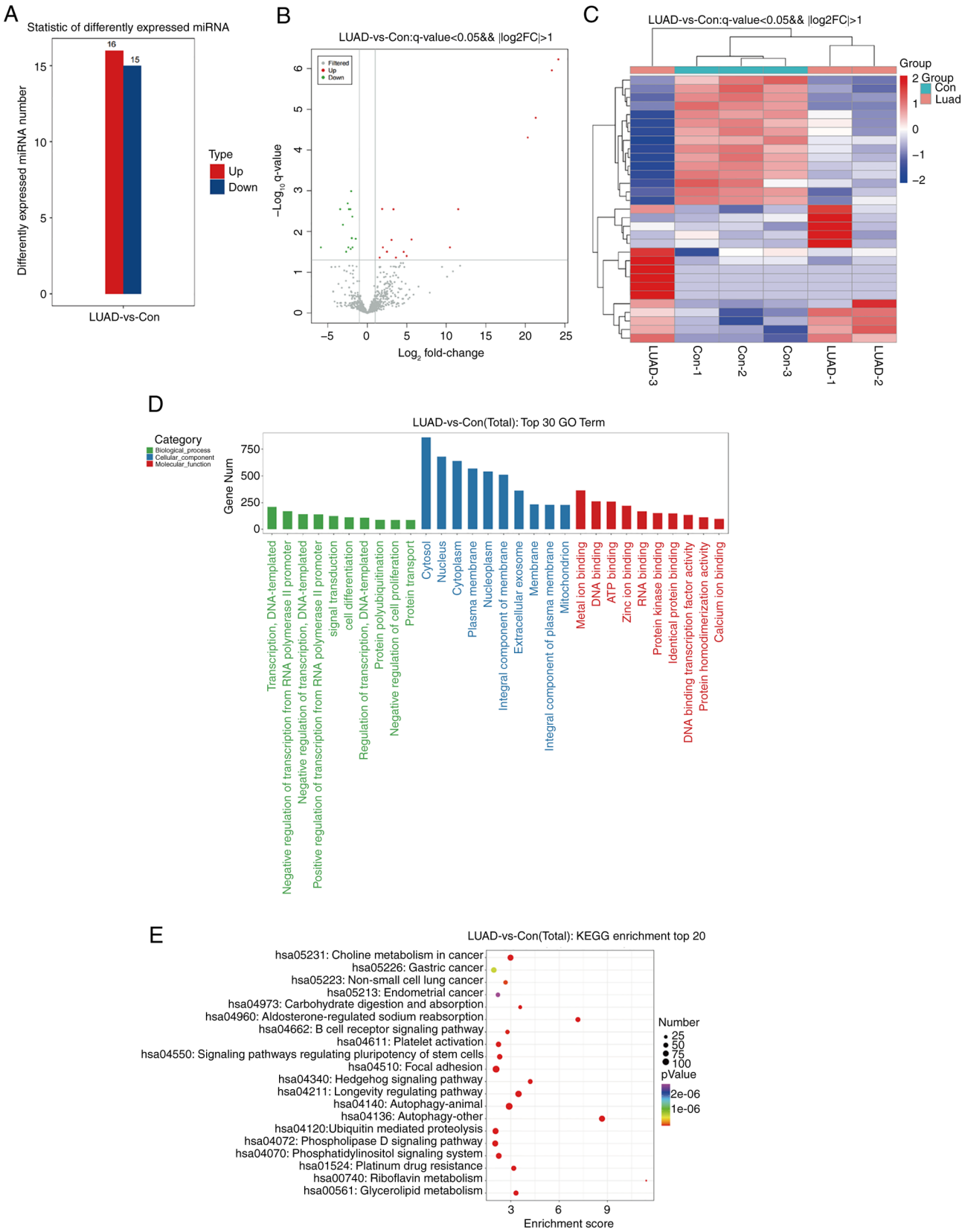

Figure 1. Screening and analysis of differential miRNAs in LUAD. (A) Differential expression mRNA number count histogram. (B) Differential expression miRNA volcano plot. (C) Heatmap depicting expression patterns of differentially expressed miRNAs. (D) Analysis of GO enrichment. (E) Exploration of KEGG pathway enrichment. miRNA, microRNA; LUAD, lung adenocarcinoma; GO, Gene Ontology; KEGG, Kyoto Encyclopedia of Genes and Genomes.

To identify target miRNAs effectively, a comprehensive search was conducted using the Starbase, Targetscan, miRWalk and miRmap databases to discover miRNAs that potentially interact with PKP3. Prior experimental data indicated a low expression of PKP3 in LUAD tissues, associating with necroptosis. Consequently, the search prioritized highly

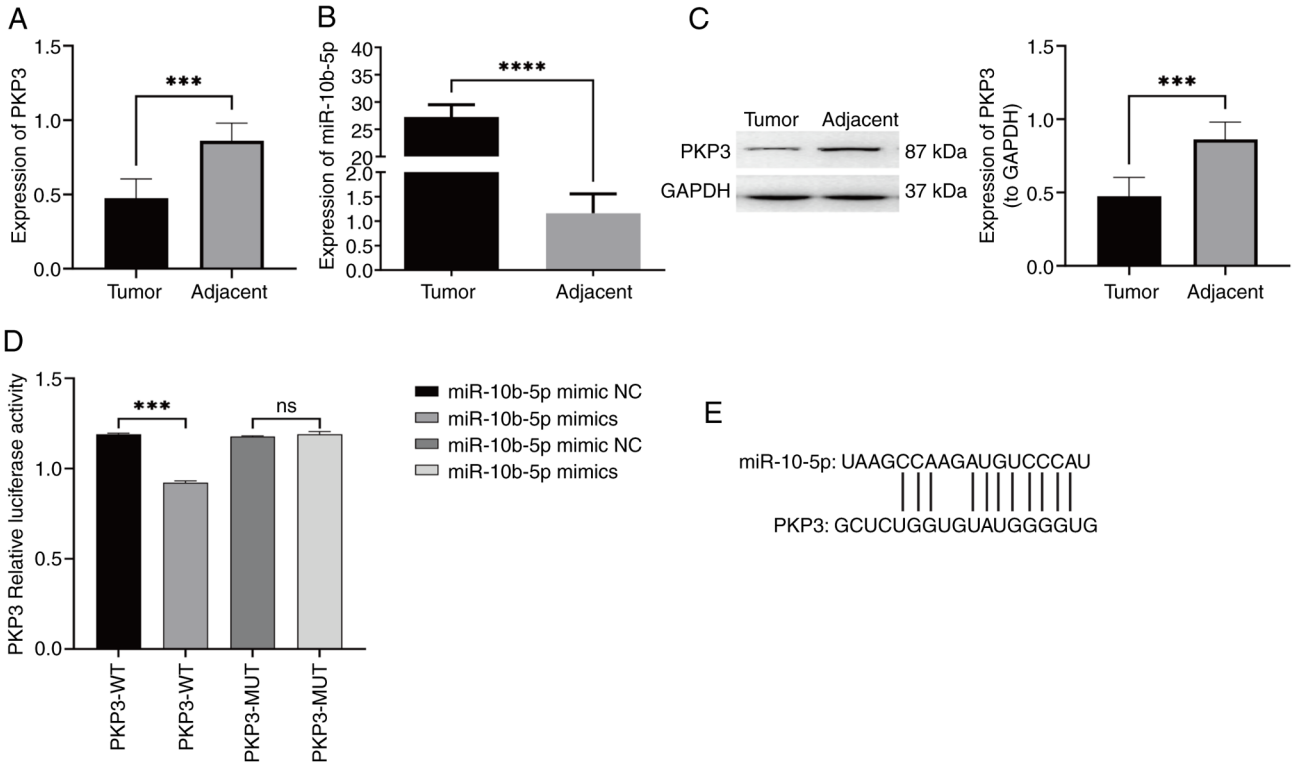

Figure 2. Examination of PKP3 and miR-10b-5p in lung adenocarcinoma along with their interaction. (A) The mRNA levels of PKP3 in tumor and corresponding non-tumor tissue were assessed using RT-qPCR. (B) RT-qPCR was utilized to determine miR-10b-5p levels in both tumor and adjacent non-tumor tissues. (C) The protein levels of PKP3 in tumor compared with adjacent tissues were analyzed through western blotting. (D) Luciferase assays, following co-transfection with PKP3-WT and PKP3-MUT in the presence of miR-10b-5p, depicted the regulatory effects through bar graphs. (E) Binding site of PKP3 to miR-10b-5p. Data represent the mean ± SD from a minimum of three independent experiments for each condition. ***P<0.001. PKP, plakophilin; miR, microRNA; RT-qPCR, reverse transcription-quantitative PCR; WT, wild-type; MUT, mutant; NC, negative control.

expressed miRNAs. Among these, only miR-10b-5p fulfilled all specified criteria, leading to its selection for subsequent clinical validation.

PKP3 is a direct regulatory target gene of miR-10b-5p. To corroborate the preliminary results and the screening of miRNAs, the expression levels of PKP3 mRNA and miR-10b-5p in LUAD tissues vs. non-tumorous counterparts were quantified using RT-qPCR (Fig. 2A and B). An analysis conducted on six paired samples indicated a significant reduction in PKP3 mRNA in LUAD tissues relative to the non-cancerous tissue, whereas miR-10b-5p showed a significant elevation. Additionally, the protein expression of PKP3 was assessed using western blot analysis in both cancerous and adjacent non-cancerous tissues (Fig. 2C). A significant reduction in PKP3 protein was observed in the LUAD samples. These results corroborate the initial data mining and sequencing findings. Further experiments involved co-transfecting A549 cells with luciferase reporter vectors embedded with either the WT PKP3 3'-UTR (PKP3-WT) or its mutant version (PKP3-MUT), along with either a miR-10b-5p mimic or mimic NC. The luminescence assay revealed diminished luciferase activity for the PKP3-WT reporter in the presence of miR-10b-5p compared with the control, a suppression that was reversed with mutations in the binding sites of PKP3 3'-UTR, indicating direct interaction and downregulation of PKP3 by miR-10b-5p (Fig. 2D). A plot of PKP3 binding site to miR-10b-5p is illustrated in Fig. 2E.

Effect of upregulation of miR-10b-5p expression on proliferation and necroptosis in LUAD cells. The investigation into the role of miR-10b-5p in LUAD involved A549 cells transfected with mimics, inhibitors, or a control vector. A total of 48 h after transfection, RT-qPCR analysis showed a significant increase in miR-10b-5p levels in cells treated with mimics compared with controls. Cells treated with inhibitors exhibited a significant reduction in miR-10b-5p, validating the efficacy of the transfection approach (Fig. 3A). A CCK-8 and cell cloning assay were conducted to evaluate the effect of miR-10b-5p level modulation on cell viability. The results revealed enhanced proliferation in cells treated with mimics and a substantial decrease in proliferation in those treated with inhibitors (Fig. 3B and C).

To investigate the role of miR-10b-5p in the process of necroptosis, A549 cells were stained with Annexin V-FITC and PI, followed by analysis via flow cytometry. This approach differentiated and quantified the cells into four categories: Viable (Annexin V-FITC-negative/PI-negative), early apoptotic (Annexin V-FITC-positive/PI-negative), late apoptotic or necrotic (Annexin V-FITC-positive/PI-positive), and non-viable (Annexin V-FITC-negative/PI-positive). The results demonstrated that the introduction of miR-10b-5p mimics did not significantly impact necroptosis compared with the control. However, interestingly, treatment of A549 cells with miR-10b-5p inhibitors significantly promoted the occurrence of necroptosis. Inhibition of miR-10b-5p led to a notable increase in necroptotic activity within A549 cells,

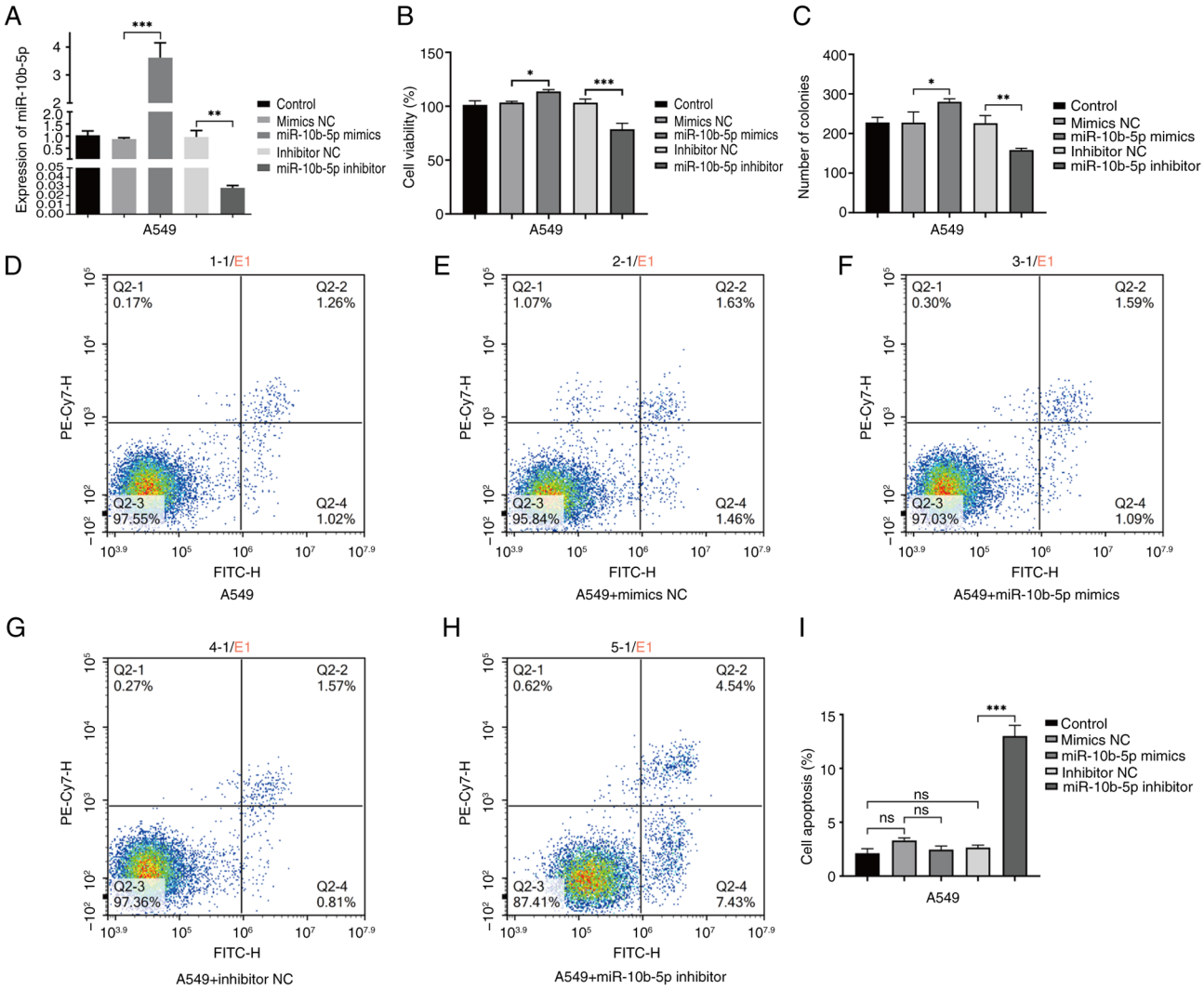

Figure 3. Examination of miR-10b-5p expression and its effects on A549 cell viability and apoptotic processes. (A) Verification of miR-10b-5p expression levels was conducted across different treatment groups in A549 cells using reverse transcription-quantitative PCR. (B) Cell viability was assessed in different A549 cell treatment groups using the Cell Counting Kit-8 assay. (C) Cell clones were assayed for cell proliferation in different A549 cell treatment groups. These groups include the control, mimics NC, miR-10b-5p mimics, inhibitor NC and miR-10b-5p inhibitor. (D-H) Flow cytometric analysis for (D) A549 cells, (E) mimics NC group, (F) miR-10b-5p mimics group, (G) inhibitor NC group and (H) miR-10b-5p inhibitor group, with Q2-2 quadrant representing late apoptotic cells and Q2-4 quadrant indicating early apoptotic cells. (I) A bar graph presents the flow cytometry findings, which are depicted as the mean ± SD from no less than three independent experiments for each group. *P<0.05, **P<0.01 and ***P<0.001. miR, microRNA; NC, negative control; ns, not significant, (P>0.05).

suggesting that miR-10b-5p inhibition promotes necroptotic processes (Fig. 3D-H).

miR-10b-5p inhibits PKP3 expression and RIPK3/MLKL signalling pathway activation and promotes Caspase-8 expression. Research indicates that upregulated miR-10b-5p facilitates proliferation while reducing necroptosis in LUAD cells. To explore the underlying molecular mechanisms of miR-10b-5p actions, the effects of both miR-10b-5p mimics and inhibitors on the expression of PKP3 and apoptosis-related genes, as well as their effects on the RIPK3/MLKL signaling pathway, were investigated using RT-qPCR and western blotting. RT-qPCR analysis indicated that miR-10b-5p mimics suppressed mRNA levels of PKP3, RIPK3 and MLKL while elevating those of Caspase-8, relative to the control. By contrast, miR-10b-5p inhibitors resulted in elevated mRNA levels of PKP3, RIPK3 and MLKL, and reduced levels of Caspase-8 (Fig. 4A-D). Western blot analysis (Fig. 4E) demonstrated a reduction in the protein levels of PKP3, p-RIPK3 and p-MLKL in the group treated with miR-10b-5p mimics relative to the control group, accompanied by an elevation in Caspase-8 protein levels. Conversely, the use of miR-10b-5p inhibitors was associated with an increase in the protein levels of PKP3, p-RIPK3 and p-MLKL, along with a reduction in Caspase-8 protein levels.

miR-10b-5p affects LUAD cell proliferation and necroptosis by regulating the PKP3/RIPK3/MLKL signalling pathway. Experimental findings suggest that an increase in miR-10b-5p expression reduces PKP3 levels and decreases activation within the RIPK3/MLKL signaling pathway, while simultaneously increasing Caspase-8 expression. To confirm that miR-10b-5p inhibits proliferation and necroptosis in LUAD cells by targeting PKP3, a stable PKP3 knockdown was established

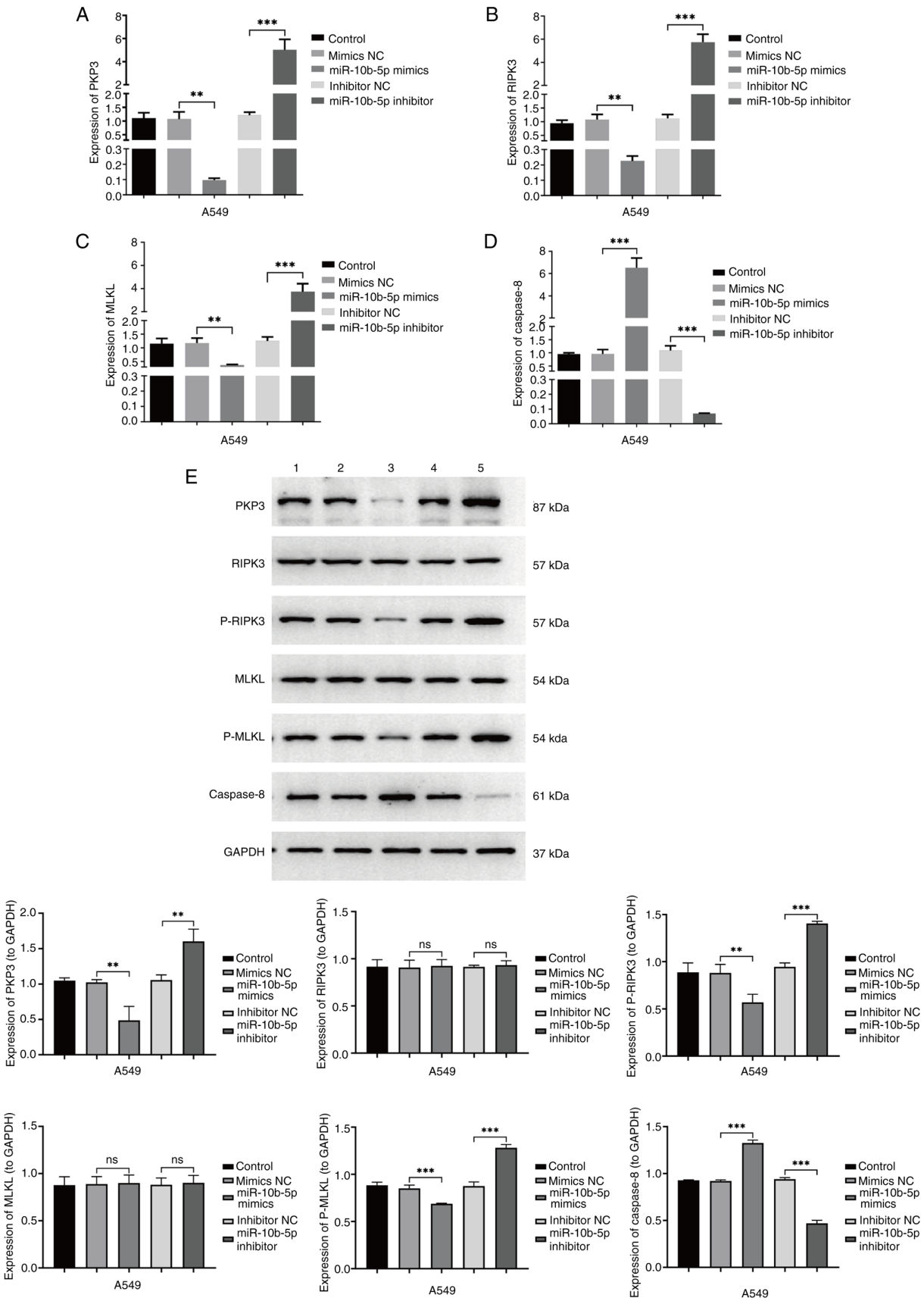

Figure 4. Effect of miR-10b-5p on A549 cellular pathways. (A) Reverse transcription-quantitative PCR confirmed PKP3 mRNA expression across various A549 cell treatment groups. (B) RIPK3 mRNA levels quantified in diverse treatment cohorts. (C) Assessment of MLKL mRNA levels in different experimental groups. (D) Analysis of caspase-8 mRNA expression among the groups. (E) Protein levels of PKP3, RIPK3, p-RIPK3, MLKL and p-MLKL, along with Caspase-8 were evaluated via western blotting in varying A549 cell treatment contexts. These groups include the A549 control, mimics NC, miR-10b-5p mimics, inhibitor NC and miR-10b-5p inhibitor. Data are presented as the mean ± SD from a minimum of three independent experiments for each group. **P<0.01 and ***P<0.001. miR, microRNA; PKP, plakophilin; RIPK, receptor-interacting protein kinase; MLKL, mixed lineage kinase domain-like protein; p-, phosphorylated; NC, negative control; ns, not significant, (P>0.05).

in the A549 cell line. RT-qPCR and western blot analysis showed significantly reduced PKP3 mRNA and protein levels in sh-PKP3 cells compared with controls (Fig. 5A and B). Functional assays, including CCK-8 and flow cytometry, indicated that miR-10b-5p inhibitor treatment significantly lowered A549 cell viability and increased apoptotic activity (Fig. 5C-I). The reduction of PKP3 mitigated the effects of the miR-10b-5p inhibitor on cell viability and apoptosis induction (Fig. 5C-I). Further qPCR analysis of mRNA levels for RIPK3, MLKL and Caspase-8 among treatment groups revealed an increase in RIPK3 and MLKL mRNA and a decrease in Caspase-8 mRNA following miR-10b-5p inhibitor treatment, an effect that was reversed with PKP3 knockdown (Fig. 5J-L). Subsequently, qPCR detected the expression of proliferation and apoptosis related genes (Fig. 5M-Q). Additionally, western blot results verified that miR-10b-5p inhibitor treatment markedly upregulated p-RIPK3, p-MLKL, Bax and Caspase-3 protein levels, while decreasing Caspase-8, proliferating cell nuclear antigen, Ki-67 and Bcl-2 protein levels, effects that were negated by PKP3 knockdown (Fig. 5R). These findings suggest that miR-10b-5p disrupts RIPK3/MLKL pathway activation by directly targeting PKP3, thereby fostering proliferation and curtailing necroptosis in A549 cells.

miR-10b-5p promotes the tumorigenic potential of LUAD cells in vivo. To investigate the role of miR-10b-5p in tumor growth *in vivo*, A549 cells were implanted, including those transfected with an inhibitor NC and a miR-10b-5p inhibitor, into the right lumbar region of nude mice at a vascular-rich site. By day 41 post-inoculation, tumors from the miR-10b-5p inhibitor cohort were significantly smaller compared with those in the control group (Fig. 6A-C). Analysis post-euthanasia revealed that suppression of miR-10b-5p led to diminished tumor growth rates relative to the controls (Fig. 6D). Subsequent studies explored the regulatory mechanisms of miR-10b-5p *in vivo*. Gene expression analysis related to apoptosis in tumor specimens was conducted via RT-qPCR and western blotting. The RT-qPCR results demonstrated a significant upregulation in the mRNA levels of PKP3, RIPK3 and MLKL in tumors treated with the miR-10b-5p inhibitor, while the mRNA levels of Caspase-8 were significantly reduced (Fig. 6E-H). Western blot analysis corroborated the increases in PKP3, p-RIPK3 and p-MLKL proteins, alongside a decrease in Caspase-8 protein levels in miR-10b-5p inhibitor-treated tumors relative to controls (Fig. 6I). TUNEL assays indicated enhanced apoptotic rates in the miR-10b-5p inhibitor-treated tumors (Fig. 6J). Enhanced necroptosis in cells from the miR-10b-5p inhibitor group compared with the control group was observed under TEM (Fig. 6K). These findings suggest that inhibiting miR-10b-5p activates the RIPK3/MLKL signaling pathway via PKP3 upregulation, leading to diminished tumor growth and increased cellular necroptosis, thereby impeding the progression of LUAD.

Discussion

Lung cancer continues to be a leading cause of cancer-related deaths, with a 5-year survival rate of only 15%, and adenocarcinoma represents the most prevalent pathological variant (26). Despite progress in immunotherapy and precision medicine, LUAD still presents significant public health issues worldwide. These challenges stem from its complex genetic diversity, common delays in diagnosis, and widespread resistance to existing medications, contributing to poor prognoses (27). In addition, gaps in knowledge concerning its pathogenesis and ongoing changes in tumor genomic expressions hinder the rapid development of effective treatments for LUAD (28). Therefore, genomic medicine is increasingly recognized as a vital area to augment and enhance research into LUAD.

Initially identified in 1993 during studies on *Cryptobacterium hidradii* nematodes (29), miRNAs are diminutive non-coding RNAs, crucial for a wide range of biological functions and diseases in various organisms. These include cell differentiation, development, aging, neurotransmission, immune reactions, apoptosis, and notably, cancer progression and tumorigenesis (30). miR-10b-5p has emerged as being significantly influential in various cancers. Research indicates that in glioblastoma, miR-10b-5p facilitates immune evasion by downregulating Ten-eleven translocation 2, which leads to decreased PD-L1 transcriptional repression (31). Another investigation revealed that in hepatocellular carcinoma, miR-10b-5p targets SLC38A2 to modulate cellular metabolism, thereby enhancing tumor growth (23). While this research offers significant insights, the exact functions and processes by which miR-10b-5p influences LUAD remain to be fully elucidated.

In the current investigation, miRNA sequencing technology was employed to identify miRNAs that are expressed differentially between LUAD and surrounding non-malignant tissues. By integrating sequencing results, initial experimental findings, and external database information, miR-10b-5p was identified. Validation confirmed that LUAD tissues exhibited reduced PKP3 expression alongside significantly elevated miR-10b-5p levels. Subsequent investigations demonstrated that the elevation in miR-10b-5p levels was a consequence of its specific interaction with the 3'-UTR of PKP3, resulting in a suppression of PKP3 expression.

Additional studies employed both enhancement and inhibition strategies to elucidate the role and mechanism of miR-10b-5p in LUAD. These experiments revealed that upregulation of miR-10b-5p promotes proliferative activity and inhibits necroptosis in A549 cells. On the other hand, downregulation of miR-10b-5p inhibited the proliferative activity and promoted necrosis in A549 cells. The dysregulated activation of the RIPK3/MLKL signaling pathway plays a crucial role in tumor progression and can trigger necroptosis (32). However, Caspase-8 has been shown to mitigate necroptosis by cleaving RIPK3 (33). The results demonstrated that miR-10b-5p overexpression led to a decrease in PKP3 levels and suppression of the RIPK3/MLKL pathway, while concurrently elevating Caspase-8 levels. By contrast, reducing miR-10b-5p expression was associated with increased PKP3 levels and activation of the RIPK3/MLKL pathway, coupled with a decrease in Caspase-8 levels.

To further examine whether miR-10b-5p exerts its necroptotic inhibitory effects in A549 cells by targeting and regulating PKP3, thereby constraining the activation of the RIPK3/MLKL pathway, PKP3 was silenced. This silencing demonstrated that the reduction of PKP3 countered the decrease in A549 cell viability and the enhancement of

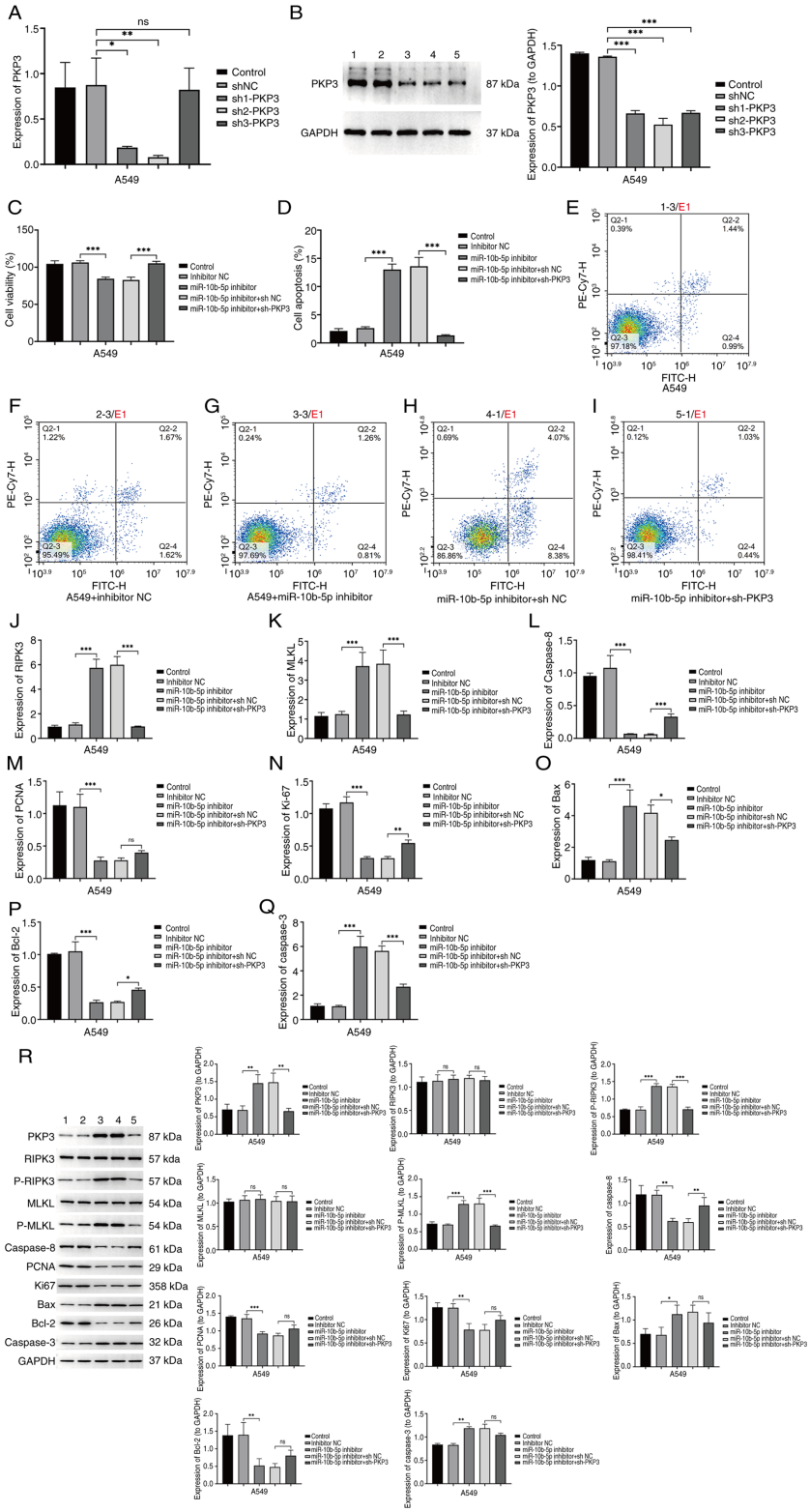

Figure 5. Modulation of cell proliferation and apoptosis via the PKP3/RIPK3/MLKL pathway (A) Validation of PKP3 mRNA levels in PKP3-silenced cells was performed by RT-qPCR. (B) PKP3 protein levels in PKP3-silenced cells were confirmed via western blotting. These groups include the control, shNC, sh1-PKP3, sh2-PKP3 and sh2-PKP3. (C) Cell Counting Kit-8 assay assessed the viability of A549 cells across various treatment groups. (D-I) Apoptotic rates in A549 cells were analyzed through flow cytometry across different treatment modalities. (D) Statistical histogram, (E) A549 group, (F) inhibitor NC group, (G) miR-10b-5p inhibitor group, (H) miR-10b-5p inhibitor + shNC group and (I) miR-10b-5p inhibitor + sh-PKP3 group. Late-stage apoptotic cells were marked in the Q2-2 quadrant, and early apoptotic cells in the Q2-4 quadrant. (J-Q) The expression levels of RIPK3, MLKL, Caspase-8, PCNA, Ki67, Bax, Bcl-2 and Caspase-3 mRNA were detected by RT-qPCR in A549 cells of different treatment groups. (R) Western blot analysis quantified PKP3 mRNA levels across varied treatment groups in A549 cells. Protein expression levels of PKP3, RIPK3, p-RIPK3, MLKL, p-MLKL, Caspase-8, PCNA, Ki67, Bax, Bcl-2 and Caspase-3 in A549 cells across the treatment groups were documented. Group identifiers included the A549 group, inhibitor NC group, miR-10b-5p inhibitor group, miR-10b-5p inhibitor + shNC group and miR-10b-5p inhibitor + sh-PKP3 group. Representative images or data are presented as the mean ± SD from a minimum of three independent experiments per group. *P<0.05, **P<0.01 and ***P<0.001. PKP, plakophilin; RIPK, receptor-interacting protein kinase; MLKL, mixed lineage kinase domain-like protein; RT-qPCR, reverse transcription-quantitative PCR; sh-, short hairpin; NC, negative control; PCNA, proliferating cell nuclear antigen; p-, phosphorylated; ns, not significant, (P>0.05).

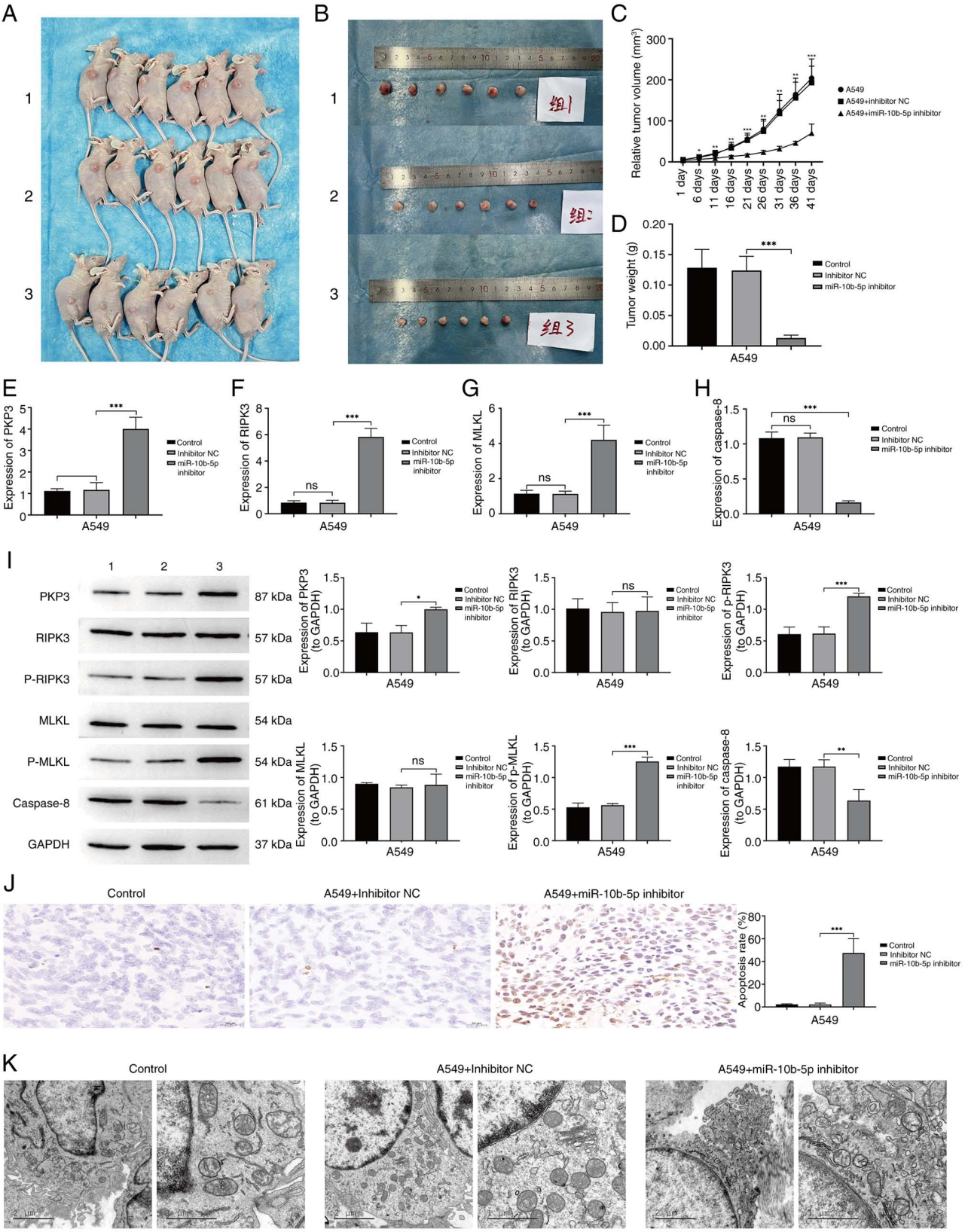

Figure 6. Effect of miR-10b-5p inhibition on the oncogenic capabilities of A549 cells *in vivo* (A-C) BALB/c nude mice were randomly assigned to receive either A549 cells, a non-specific control inhibitor, or miR-10b-5p inhibitor-treated A549 cells. By day 41 post-inoculation, tumors in the miR-10b-5p inhibitor group exhibited a significant reduction in size compared with the other groups. (D) Graph depicting tumor growth trajectories following cell inoculation. (E-H) Expression levels of (E) PKP3, (F) RIPK3, (G) MLKL and (H) Caspase-8 were quantified by reverse transcription-quantitative PCR across the various treatment cohorts. (I) Western blot analysis was conducted to quantify the protein levels of PKP3, RIPK3, p-RIPK3, MLKL, p-MLKL and Caspase-8 across different treatment groups. (J) Apoptosis in cells from different treatment groups was assessed using TUNEL staining. (K) Transmission electron microscopy provided visual evidence of cellular morphology across the treatment groups. Group designations were as follows: A549 group, inhibitor NC group, and miR-10b-5p inhibitor group. Data are presented as the mean ± SD, derived from a minimum of three independent experiments for each group. *P<0.05, **P<0.01 and ***P<0.001. miR, microRNA; PKP, plakophilin; RIPK, receptor-interacting protein kinase; MLKL, mixed lineage kinase domain-like protein; p-, phosphorylated; NC, negative control; ns, not significant, (P>0.05).

necroptosis initially induced by miR-10b-5p knockdown. In a similar fashion, reducing PKP3 levels mitigated the enhanced activation of the RIPK3/MLKL pathway due to miR-10b-5p suppression. These findings suggest that miR-10b-5p mitigates apoptosis in LUAD cells by targeting PKP3, leading to suppressed activation of the RIPK3/MLKL pathway. Additional *in vivo* validations were conducted, revealing that miR-10b-5p knockdown curbed LUAD progression and enhanced necroptosis via the PKP3-mediated activation of the RIPK3/MLKL pathway.

In conclusion, through *in vivo* and *ex vivo* experiments, it was found for the first time to the best of our knowledge, that miR-10b-5p, as an oncogene, promotes the proliferation of LUAD cells and inhibits necroptosis by suppressing PKP3-mediated activation of the RIPK3/MLKL signalling pathway. Notably, knockdown of miR-10b-5p inhibited LUAD development by promoting the onset of necroptosis. In addition, the present study has certain limitations. The sample size was small, only 6 cases, which may affect the wide applicability of the results and the reliability of statistical analyses, but a large number of experiments were conducted at a later stage to prove and validate them. In conclusion, the current findings provide new insights into the mechanisms of LUAD progression and suggest that targeting miR-10b-5p has the potential to be a new effective therapeutic tool.

Acknowledgements

Not applicable.

Funding

The present study was supported by the Yunnan health training project of high-level talents (grant no. D-2018041).

Availability of data and materials

The data generated in the present study may be requested from the corresponding author.

Authors' contributions

YH, XL, ZY, RM, YW, GY and JH contributed to the study conception and design, prepared materials, collected and analyzed the data. YH and ZY wrote the first draft of the manuscript. YW and GY confirm the authenticity of all the raw data. All authors read and approved the final version of the manuscript.

Ethics approval and consent to participate

The research protocols for human studies adhered to the ethical guidelines of the Declaration of Helsinki and were approved by The Second Affiliated Hospital of Kunming Medical University (KMUH) Ethics Committee (approval no. PJ-2024-125; Kunming, China). Written informed consent was obtained from all participants. Animal experimental protocol was approved by the KMUH Animal Care Committee (approval no. kyfeyxm2024127; Kunming, China).

Patient consent for publication

Not applicable.

Competing interests

The authors declare that they have no competing interests.

References

1. Zhao B, Xu H, Ai X, Adalat Y, Tong Y, Zhang J and Yang S: Expression profiles of long noncoding RNAs in lung adenocarcinoma. Onco Targets Ther 11: 5383-5390, 2018.
2. Wei X, Li X, Hu S, Cheng J and Cai R: Regulation of ferroptosis in lung adenocarcinoma. Int J Mol Sci 24: 14614, 2023.
3. Denisenko TV, Budkevich IN and Zhivotovsky B: Cell death-based treatment of lung adenocarcinoma. Cell Death Dis 9: 117, 2018.
4. Chen H, Xia R, Jiang L, Zhou Y, Xu H, Peng W, Yao C, Zhou G, Zhang Y, Xia H and Wang Y: Overexpression of RhoV promotes the progression and EGFR-TKI resistance of lung adenocarcinoma. Front Oncol 11: 619013, 2021.
5. Li S, Choi YL, Gong Z, Liu X, Lira M, Kan Z, Oh E, Wang J, Ting JC, Ye X, *et al*: Comprehensive characterization of oncogenic drivers in asian lung adenocarcinoma. J Thorac Oncol 11: 2129-2140, 2016.
6. Zhang Y, Chen J, Tian J, Zhou Y and Liu Y: Role and function of plakophilin 3 in cancer progression and skin disease. Cancer Sci 115: 17-23, 2024.
7. Du Y, Hou S, Chen Z, Li W, Li X and Zhou W: Comprehensive analysis identifies PKP3 overexpression in pancreatic cancer related to unfavorable prognosis. Biomedicines 11: 2472, 2023.
8. Lim V, Zhu H, Diao S, Hu L and Hu J: PKP3 interactions with MAPK-JNK-ERK1/2-mTOR pathway regulates autophagy and invasion in ovarian cancer. Biochem Biophys Res Commun 508: 646-653, 2019.
9. Liu B, Feng Y, Xie N, Yang Y and Yang D: FERMT1 promotes cell migration and invasion in non-small cell lung cancer via regulating PKP3-mediated activation of p38 MAPK signaling. BMC Cancer 24: 58, 2024.
10. Lee LYW, Woolley C, Starkey T, Biswas S, Mirshahi T, Bardella C, Segditsas S, Irshad S and Tomlinson I: Serum- and Glucocorticoid-induced kinase sgk1 directly promotes the differentiation of colorectal cancer cells and restrains metastasis. Clin Cancer Res 25: 629-640, 2019.
11. Takahashi H, Nakatsuji H, Takahashi M, Avirmed S, Fukawa T, Takemura M, Fukumori T and Kanayama H: Up-regulation of plakophilin-2 and Down-regulation of plakophilin-3 are correlated with invasiveness in bladder cancer. Urology 79: 240.e1-e8, 2012.
12. Furukawa C, Daigo Y, Ishikawa N, Kato T, Ito T, Tsuchiya E, Sone S and Nakamura Y: Plakophilin 3 oncogene as prognostic marker and therapeutic target for lung cancer. Cancer Res 65: 7102-7110, 2005.
13. Liu Z, Wang T, She Y, Wu K, Gu S, Li L, Dong C, Chen C and Zhou Y: N6-methyladenosine-modified circIGF2BP3 inhibits CD8+ T-cell responses to facilitate tumor immune evasion by promoting the deubiquitination of PD-L1 in non-small cell lung cancer. Mol Cancer 20: 105, 2021.
14. Kim HJ, Roh MS, Son CH, Kim AJ, Jee HJ, Song N, Kim M, Seo SY, Yoo YH and Yun J: Loss of Med1/TRAP220 promotes the invasion and metastasis of human non-small-cell lung cancer cells by modulating the expression of metastasis-related genes. Cancer Lett 321: 195-202, 2012.
15. Qin X, Ma D, Tan YX, Wang HY and Cai Z: The role of necroptosis in cancer: A double-edged sword? Biochim Biophys Acta Rev Cancer 1871: 259-266, 2019.
16. Zhu F, Zhang W, Yang T and He SD: Complex roles of necroptosis in cancer. J Zhejiang Univ Sci B 20: 399-413, 2019.
17. Philipp S, Sosna J and Adam D: Cancer and necroptosis: Friend or foe? Cell Mol Life Sci 73: 2183-2193, 2016.
18. Hayes J, Peruzzi PP and Lawler S: MicroRNAs in cancer: Biomarkers, functions and therapy. Trends Mol Med 20: 460-469, 2014.
19. Su Z, Yang Z, Xu Y, Chen Y and Yu Q: MicroRNAs in apoptosis, autophagy and necroptosis. Oncotarget 6: 8474-8490, 2015.

20. Harari-Steinfeld R, Gefen M, Simerzin A, Zorde-Khvalevsky E, Rivkin M, Ella E, Friehmann T, Gerlic M, Zucman-Rossi J, Caruso S, *et al*: The lncRNA H19-Derived MicroRNA-675 promotes liver necroptosis by targeting FADD. Cancers (Basel) 13: 411, 2021.
21. Li X, Tibenda JJ, Nan Y, Huang SC, Ning N, Chen GQ, Du YH, Yang YT, Meng FD and Yuan L: MiR-204-3p overexpression inhibits gastric carcinoma cell proliferation by inhibiting the MAPK pathway and RIP1/MLK1 necroptosis pathway to promote apoptosis. World J Gastroenterol 29: 4542-4556, 2023.
22. Yan T, Wang X, Wei G, Li H, Hao L, Liu Y, Yu X, Zhu W, Liu P, Zhu Y and Zhou X: Exosomal miR-10b-5p mediates cell communication of gastric cancer cells and fibroblasts and facilitates cell proliferation. J Cancer 12: 2140-2150, 2021.
23. Xia M, Chen J, Hu Y, Qu B, Bu Q and Shen H: miR-10b-5p promotes tumor growth by regulating cell metabolism in liver cancer via targeting SLC38A2. Cancer Biol Ther 25: 2315651, 2024.
24. Li S, Mao L, Song L, Xia X, Wang Z, Cheng Y, Lai J, Tang X and Chen X: Extracellular vesicles derived from glioma stem cells affect glycometabolic reprogramming of glioma cells through the miR-10b-5p/PTEN/PI3K/Akt pathway. Stem Cell Rev Rep 20: 779-796, 2024.
25. Livak KJ and Schmittgen TD: Analysis of relative gene expression data using real-time quantitative PCR and the 2(-Delta Delta C(T)) method. Methods 25: 402-408, 2001.
26. Song Y, Kelava L and Kiss I: MiRNAs in lung adenocarcinoma: Role, diagnosis, prognosis, and therapy. Int J Mol Sci 24: 13302, 2023.
27. Liu J, Zhang F, Wang J and Wang Y: MicroRNA-mediated regulation in lung adenocarcinoma: Signaling pathways and potential therapeutic implications (Review). Oncol Rep 50: 211, 2023.
28. Molina JR, Yang P, Cassivi SD, Schild SE and Adjei AA: Non-small cell lung cancer: Epidemiology, risk factors, treatment, and survivorship. Mayo Clin Proc 83: 584-594, 2008.
29. Lee RC, Feinbaum RL and Ambros V: The C. elegans heterochronic gene lin-4 encodes small RNAs with antisense complementarity to lin-14. Cell 75: 843-854, 1993.
30. Ambros V: The functions of animal microRNAs. Nature 431: 350-355, 2004.
31. Du W, Chen D, Wei K, Yu D, Gan Z, Xu G and Yao G: MiR-10b-5p impairs TET2-Mediated inhibition of PD-L1 transcription thus promoting immune evasion and tumor progression in glioblastoma. Tohoku J Exp Med 260: 205-214, 2023.
32. Zhou Y, Xiang Y, Liu S, Li C, Dong J, Kong X, Ji X, Cheng X and Zhang L: RIPK3 signaling and its role in regulated cell death and diseases. Cell Death Discov 10: 200, 2024.
33. Yuan J and Ofengeim D: A guide to cell death pathways. Nat Rev Mol Cell Biol 25: 379-395, 2024.